

# The effect of oxide and tribofilm formation on the wear of cylinder bores from flex-fuel engines

Obara, R.B.<sup>1,2</sup>, Faria, J.O.M.G.<sup>3</sup>, Sinatora, A.<sup>2</sup>,

<sup>1</sup>Tupy S.A.

<sup>2</sup>Escola Politécnica da Universidade de São Paulo

<sup>3</sup>Instituto de Pesquisas Tecnológicas do Estado de São Paulo

Copyright © 2016 SAE International

## Abstract

It is well known that machine lifetime, reliability and performance are strongly related to wear. The wear of cylinder bores can increase blow-by, oil consumption, power losses and emissions. Moreover, it can produce axial wear scratches that can harm hydrodynamic support of piston rings, increasing wear even further. The comprehension of the main factors responsible for wear in cylinder bores is, therefore, indispensable for the increase of the efficiency of engines. Despite the great work reported in literature regarding to the analysis of wear in engine cylinders, the study of the types of oxides and tribofilms formed in the surface of the cylinders remains poor. Therefore, the present work aims to correlate wear of cylinder bores from flex-fuel vehicles with engine operating conditions. Although most publications show that top dead center (TDC) is the region of the cylinder with highest wear rates, the present work shows favorable conditions to the formation of certain oxides and tribofilms capable to minimize wear of TDC, making it even lower than the wear usually experienced by bottom dead center (BDC).

## Introduction

Driven by stricter governmental legislations and increasingly demanding markets, automakers and original equipment manufacturers (OEMs) have developed new engine technologies capable of increasing engine performance by reducing pollutant emissions, oil consumption and power losses. Several solutions have been proposed, but some tribological problems have arisen from them. Engine temperature has increased due to turbocharging, oil viscosity has decreased [1-4], exhaust gas recirculation (EGR) has been widely used to reduce NOx emissions and ethanol has also been used in high concentrations in flexible fuel vehicles in Brazil, North America and Sweden. Despite the great advantages from these technologies, they can contribute for the intensification of oxidative wear in engine components.

Higher temperatures and loads inside the combustion chamber associated to the use of low viscosity lubricants can lead to oil film break down, increasing the tendency to oxidation [5]. The condensation of the moisture present in recirculated exhaust gases and the water contamination of ethanol can both increase the corrosion in combustion chamber [6-10]. Direct injection of ethanol can even worsen corrosion of engine parts. Therefore, one can notice the great tribological challenges existing in flex-fuel engines.

Classical and recent publications agree that oxidative wear is one of the most important wear mechanisms in cylinder bores for both Otto and Diesel cycle engines [11-14]. If we consider that the wear of cylinder bores is closely related to the increase in oil consumption, pollutant emissions and power losses, one can notice that the comprehension of oxidative wear in internal combustion engines has a great potential for increasing engine lifetime, reliability and performance.

Oxide formation can increase or decrease friction and wear depending on its hardness and adherence to the substrate [15]. Bisson [16] showed that films of graphitic carbon on cast irons, wüstite (FeO) and magnetite (Fe<sub>3</sub>O<sub>4</sub>) can reduce friction and wear on ferrous materials, while abrasive films such as hematite (Fe<sub>2</sub>O<sub>3</sub>) have detrimental tribological properties. Regarding to iron oxides, Hutchings [15] states that Fe<sub>2</sub>O<sub>3</sub> dominates at low speeds and temperatures, while FeO is formed at high speeds and temperatures. Under intermediate conditions, Fe<sub>3</sub>O<sub>4</sub> predominates. It is well known that temperature is the most important variable affecting oxidation rate and oxide composition. Therefore, the wide range of speeds and temperatures inside the cylinder bore – responsible for the occurrence of different lubricating regimes and wear mechanisms [17, 18] – can give rise to several types of oxides and tribofilms with different tribological properties.

Besides the importance of bulk temperature – which is very important for static oxidation – local temperature at the interface (flash temperature) due to friction power dissipation

can also be responsible for oxide formation and wear [15, 19]. Kennedy [20] observed flash temperatures much higher than the contact (or nominal) temperature for lubricated and unlubricated sliding wear. While nominal contact temperature is usually lower than 500°C [21], thermoelectric and pyrometry measurements show that flash temperature rises may exceed 1100°C [15, 22]. Therefore, both the temperature distribution within the cylinder and the piston dynamic can affect the formation of oxide films.

Due to the great effect of oxide and tribofilm formation in terms of friction and wear, the present study aims to correlate oxide and tribofilm formation with engine operating conditions and, thereafter, with the wear of the cylinder bores from flex-fuel engines.

## Materials and Methods

In this work, a typical 1.4 L flex-fuel engine from Brazilian market with 4 cylinders in line was tested in vehicle. Table 1 shows the chemical composition of the gray cast iron cylinder liners.

A Horiba XploRA ONE Raman spectrometer with 532 nm DPSS laser equipped with a 1200 lines per mm grating was used to characterize oxides and tribofilms. A Taylor Hobson CCI MP optical profilometer was used to analyze the topography of the cylinder bore and to quantify its wear by the assessment of volume losses. The region below the bottom dead center (BDC) was used as a reference height, since it does not wear out.

The contact temperature was obtained by summing bulk and flash temperatures, as shown in Equation 1.

$$T_c = T_b + \Delta T_f \quad (1)$$

Flash temperature for line contact was obtained by employing the Jaeger formulas [23]:

$$\Delta T_{f_{ring}} = 0.399 \frac{\mu W |U_p - U_c|}{Kl} \left( \frac{\chi}{Ub} \right)^{0.5} \quad (2)$$

$$\Delta T_{f_{cylinder}} = \frac{4\chi q}{\pi K U} (-2,303L \log_{10} L + 1.116L) \quad (3)$$

$$\frac{1}{\Delta T_f} = \frac{1}{\Delta T_{f_{ring}}} + \frac{1}{\Delta T_{f_{cylinder}}} \quad (4)$$

where  $\mu$  is the coefficient of friction,  $W$  is the normal load [N],  $U_p$  and  $U_c$  are the surface velocities for piston and cylinder [m/s],  $K$  is the thermal conductivity [W/mK],  $l$  is the half length of the contact rectangle [m],  $\chi$  is the thermal diffusivity [m<sup>2</sup>/s],  $U$  is the velocity for piston or cylinder,  $b$  is the half width of the contact rectangle [m],  $q = \mu W |U_p - U_c| / (4bl)$  is the rate of heat supply per unit area [W/m<sup>2</sup>] and  $L = Ub / (2\chi)$  is the Peclet number.

Oxide composition was estimated by using the software FactSage 7.0.

## Results and Analysis

The pressure-crank angle diagram (Fig. 1) was used to estimate contact pressures between compression ring and cylinder bore during the power stroke assuming that the pressure behind the first compression ring varies according to the cylinder pressure [18]. Fig. 2 shows the calculated contact temperatures for top and bottom dead centers (0° and 180°, respectively). Even though Jaeger formulas cannot be applied to estimate contact temperatures for hydrodynamic lubrication, a dashed line was added in Fig.2 to show that cylinder temperature tends to decrease when relatively thick oil films prevent metal-to-metal contact.

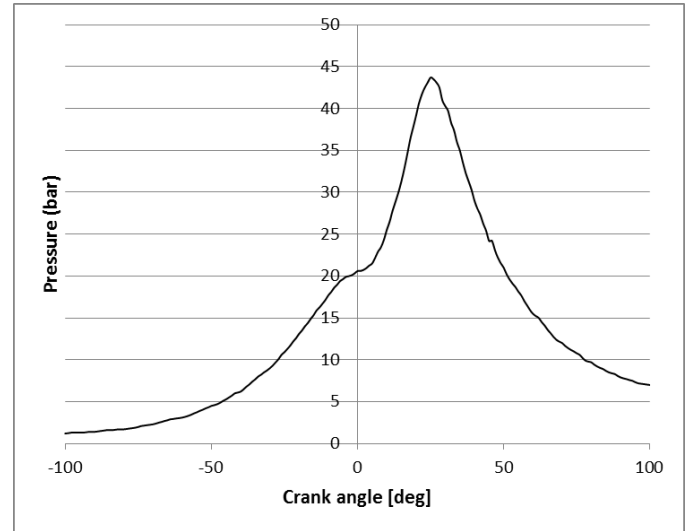


Figure 1. Pressure-crank angle diagram for compression and power strokes (1300 rpm).

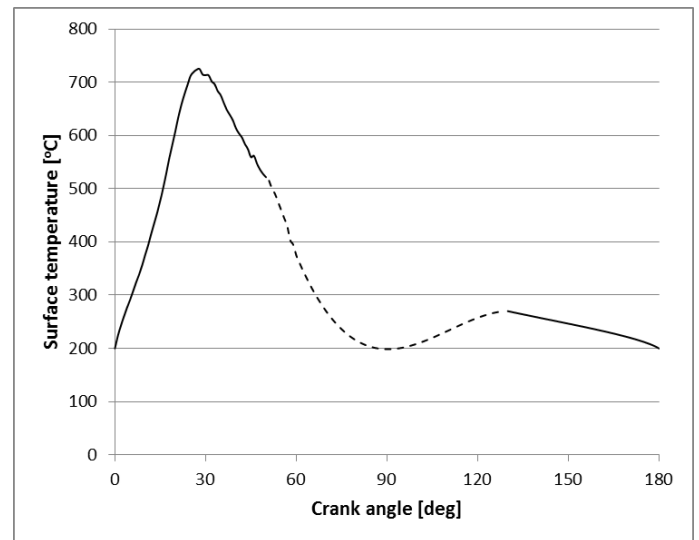


Figure 2. Temperature of the cylinder during power stroke.

Fig. 3 shows the simulation for oxide composition at 200°C and 700°C. As can be seen, for reducing atmospheres and high temperatures wüstite (FeO) dominates, while hematite (Fe<sub>2</sub>O<sub>3</sub>) is formed for oxidant atmospheres. Under intermediate conditions, magnetite (Fe<sub>3</sub>O<sub>4</sub>) is formed. Reducing and oxidant atmospheres alternate at each stroke of the engine. Also, combustion produces water, which promotes the formation of hematite [15].

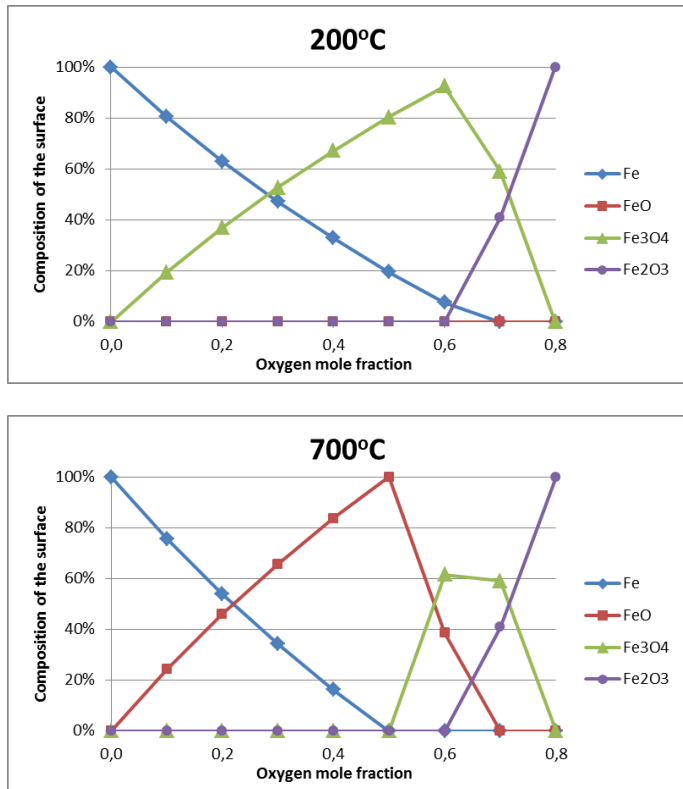


Figure 3. Estimation of oxide composition.

Jaeger and Archard flash-temperature models for high-speed sliding [23, 24] indicates that the maximum flash temperature is inversely proportional to the real contact area divided by  $\sqrt{b}$  (or by the square root of the radius, for circular contacts). Since real contact area can vary substantially with surface finishing, material properties at the working temperature and contact pressures [25, 26], these may be the main factors affecting oxide and tribofilm formation in cylinder bores from internal combustion engines.

Even though flash-temperature models do not allow a precise estimation of contact temperatures [27, 28], they can be used to indicate trends and, as can be seen in Fig.2, higher contact temperatures are expected to be found at TDC. That was

exactly the region of the cylinder bore with higher concentration of corrosion pits (Fig. 4), suggesting that oxidation preferably occurred for higher contact pressures and temperatures.

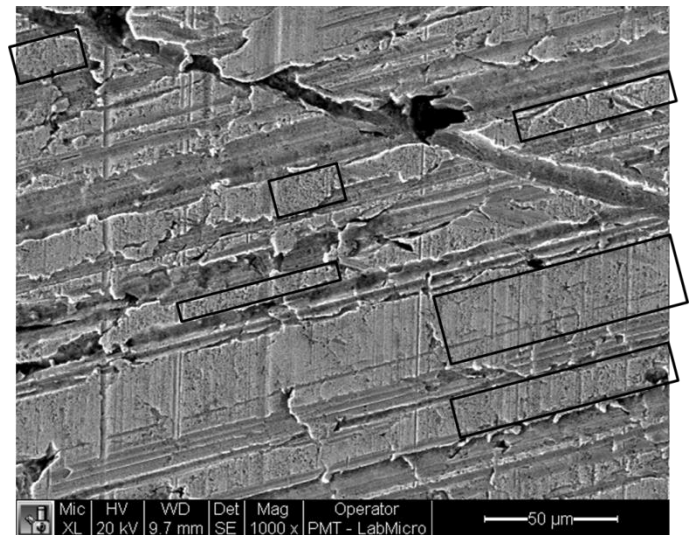


Figure 4. TDC of the honed surface showing corrosion pits.

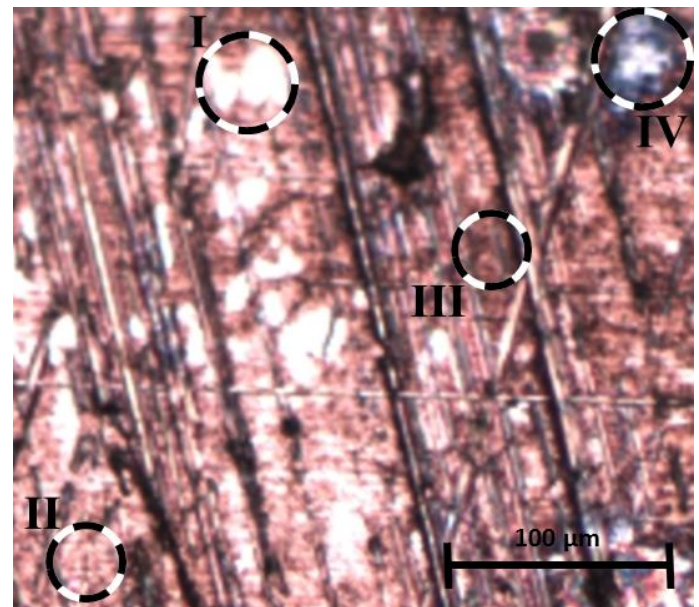


Figure 5. Positions at TDC in which oxides and tribofilms were analyzed (10x amplification).

Table 1. Chemical composition of the cylinder liner.

C	Si	Mn	P	S	Cr	Ti	Sn	Cu	Pb	Al
3,34%	2,53%	0,827%	0,339%	0,050%	0,473%	0,017%	0,005%	0,018%	0,002%	0,004%

## Characterization of Oxides

Raman spectroscopy was used to study oxide and tribofilm formation at top and bottom dead centers and in the mid-stroke region of the cylinder. Figs. 5-7 show the analyzed positions for each region of the cylinder bore.

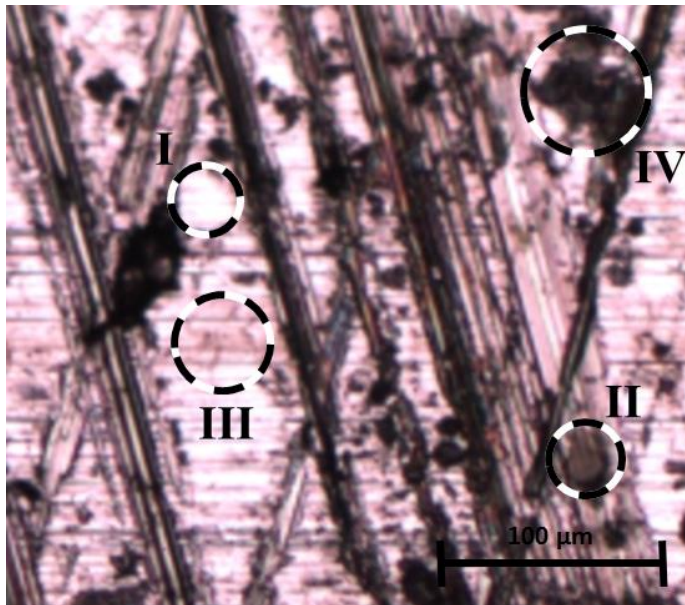


Figure 6. Positions in the mid-stroke region of the cylinder in which oxides and tribofilms were analyzed (10x amplification).

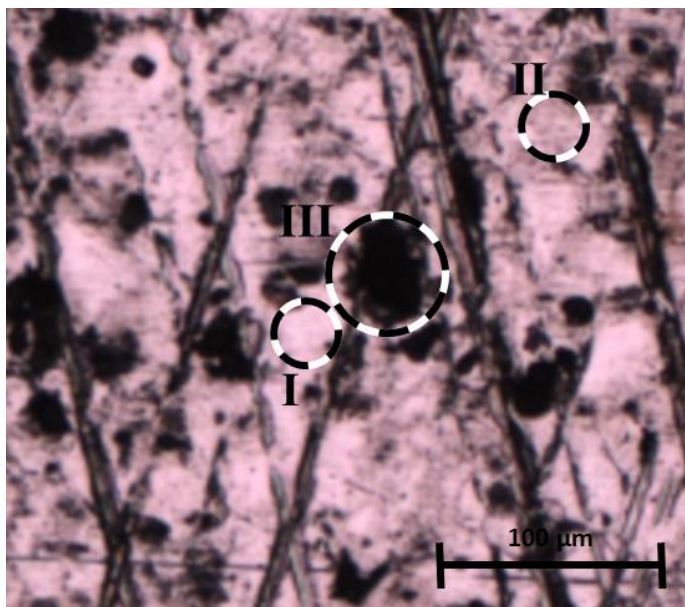


Figure 7. Positions at BDC in which oxides and tribofilms were analyzed (10x amplification).

Fig. 8 shows Raman spectra at TDC for Raman shifts 100-1200  $\text{cm}^{-1}$  and 1200-2000  $\text{cm}^{-1}$ . The spectra were split into two single graphs to ease the study of oxides and carbon tribofilms

separately. Raman spectra for magnetite, graphite and graphite tribofilm were added as a reference for comparison. All reference spectra were obtained for a laser excitation wavelength at 532 nm. Graphitic materials present the so-called D band at 1350  $\text{cm}^{-1}$ , the G band at 1582  $\text{cm}^{-1}$  and the D' band at 1620  $\text{cm}^{-1}$  [29]. The D' band and the ratio of the D and G band intensities are both related to any kind of disorder or defects in the graphitic structure [29-31]. In addition to the above mentioned bands for graphite, Raman spectrum of graphite tribofilm may present vibration frequencies centered at about 1430  $\text{cm}^{-1}$ , which can be explained by the chemisorption of hydrogen on graphite [32-34]. Analyzing the Raman spectrum for the four selected regions at TDC, one can notice that the higher temperatures and contact pressures at TDC gave rise to the formation of magnetite in the darker regions of Fig. 5. Also, with exception of the white region, all the others presented the formation of a graphite tribofilm with relatively small amount of defects.

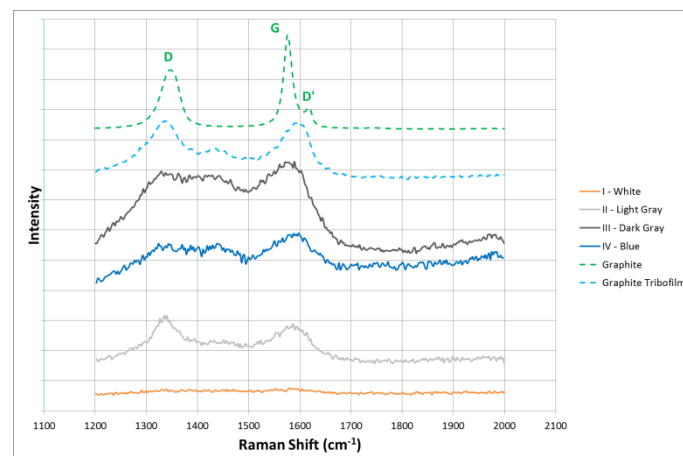
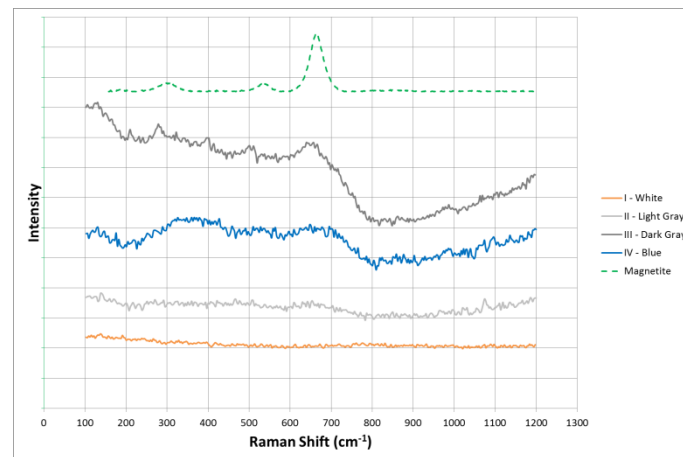


Figure 8. Raman spectra at TDC.

Fig. 9 shows Raman spectra for the selected positions of the mid-stroke region of the cylinder. Position III presented the formation of magnetite and relatively ordered graphite tribofilm, while positions II and IV presented the formation of hematite and a highly disordered graphite tribofilm.

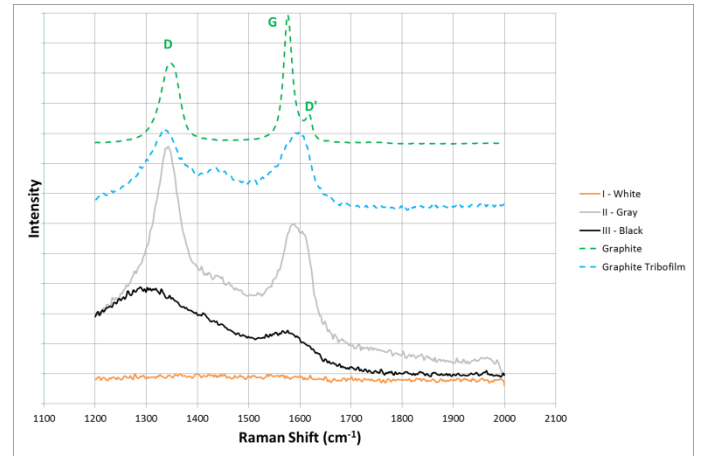
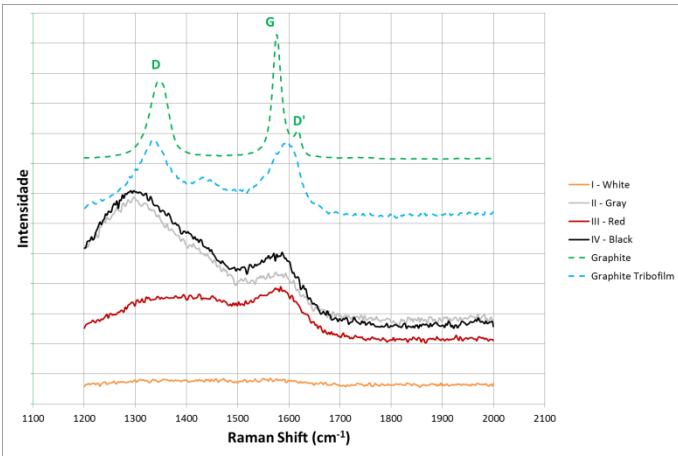
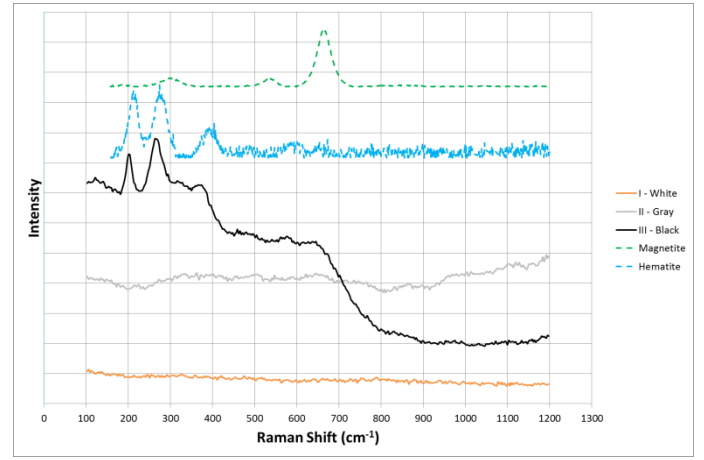
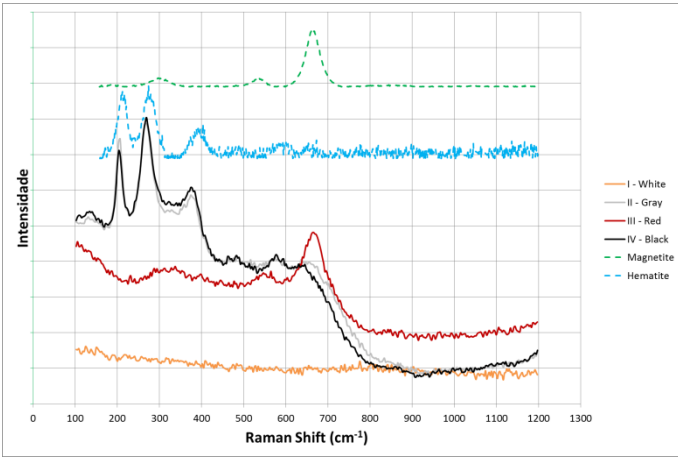


Figure 9. Raman spectra in the mid-stroke region of the cylinder.

Figure 10. Raman spectra at BDC.

Fig. 10 shows Raman spectra at BDC. One can notice the presence of hematite and a highly disordered graphite tribofilm. No evidences of magnetite formation were found.

Wear was computed by comparing the heights of worn and unworn regions. One can notice lower wear rates in the mid-stroke region of the liner – which occur due to hydrodynamic lubrication, preventing metal-to-metal contact – and higher wear at BDC – which can be confirmed by the lower roughness of plateau (Sk) and peaks (Spk) averaged along this region.

### Quantification of Wear

3D topographies were obtained from TDC to the region below BDC with certain overlap between them and an algorithm for relocation [35] was implemented in Matlab to precisely join the topographies (Fig. 11). During the stitching operation, one topography was moved relative to the other and the cross-correlation coefficient was calculated. The perfect alignment between the common areas corresponds to the minimum value for the cross-correlation coefficient, which can be given by:

$$c = \frac{\sum_{i,j} [(x_A - x_A^m)(x_B - x_B^m)](i,j)}{\sqrt{[\sum_{i,j} (x_A(i,j) - x_A^m)^2][\sum_{i,j} (x_B(i,j) - x_B^m)^2]}} \quad (5)$$

where  $A$  and  $B$  are the indexes of the analyzed topographies,  $x_A(i,j)$  and  $x_B(i,j)$  are the  $z$  coordinates for the position  $(i,j)$  of topographies  $A$  and  $B$  and  $x_A^m$  and  $x_B^m$  are the average values for topographies  $A$  and  $B$ , so that  $x^m = [\sum_i^n \sum_j^m (x_{i,j})] / (n \times m)$ .

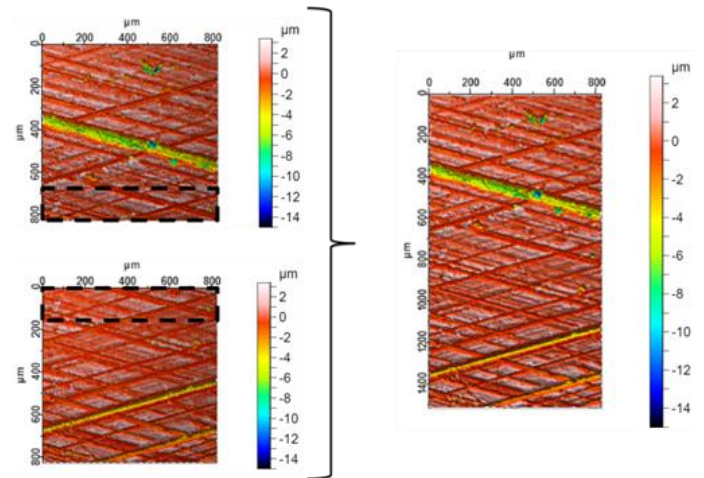


Figure 11. Stitching operation to join the surfaces.

Fig. 12 shows the profile of the cylinder bore after stitching all the topographies. As can be seen, the wear process created a step between BDC and the unworn region of the cylinder.

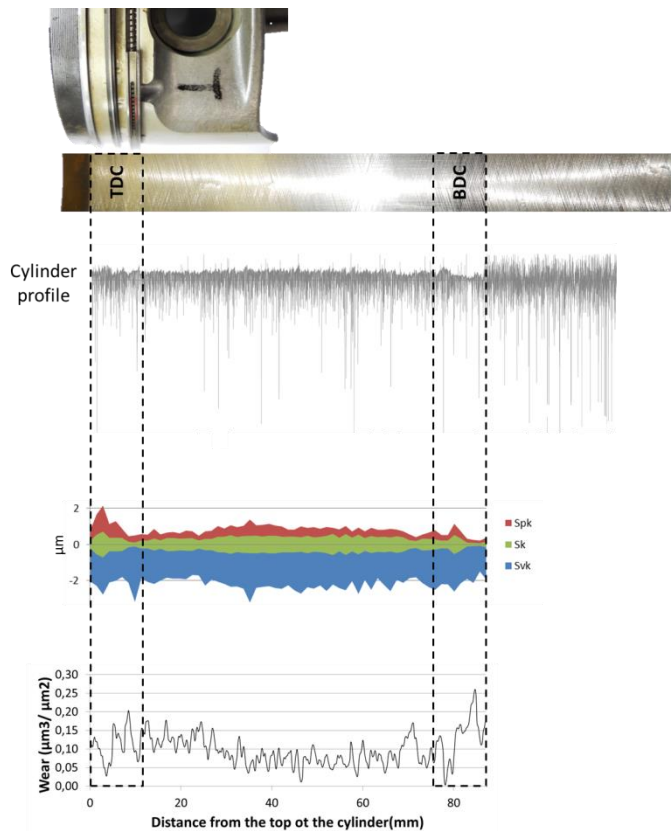


Figure 12. Cylinder profile, variation of Sk family parameters and wear.

## Conclusions

Temperature, contact pressures and oxygen availability vary several times per second during engine normal operation, making oxide and tribofilm estimation a hard task. Nonetheless, the present work has shown that local contact conditions – which are strongly related to both the roughness of cylinder bore and temperature/pressure inside the combustion chamber – are the main factors affecting oxide and tribofilm formation in cylinder bores from internal combustion engines.

In the present work, a flex-fuel engine was analyzed in terms of quantification of wear and characterization of oxides and tribofilms. Although literature indicates that higher wear rates are expected to be found at TDC [14, 36, 37], the analyzed flex-fuel engine surprisingly presented higher wear at BDC. Raman spectroscopy analysis revealed that magnetite and more ordered graphite tribofilm were more likely to be found in the top region of the cylinder. Therefore, the low shear strength from magnetite and  $sp^2$  carbon networks may have prevented scuffing and reduced friction and wear at this portion of the cylinder. On the other hand, hematite and more disordered graphite tribofilm were essentially found closer to BDC (where wear rates achieved its maximum value). These factors may have increased abrasive wear and enhanced the propensity for scuffing, increasing both friction and wear [15, 38].

## References

1. Manni, M., and Florio, S., 2013, "An Experimental Evaluation of the Impact of Ultra Low Viscosity Engine Oils on Fuel Economy and CO<sub>2</sub> Emissions," No. 0148-7191, SAE Technical Paper.
2. Okuyama, Y., Shimokoji, D., Sakurai, T., and Maruyama, M., 2011, "Study of low-viscosity engine oil on fuel economy and engine reliability," No. 0148-7191, SAE Technical Paper.
3. Tanaka, H., Nagashima, T., Sato, T., and Kawauchi, S., 1999, "The effect of 0W-20 low viscosity engine oil on fuel economy," No. 0148-7191, SAE Technical Paper.
4. Ushioda, N., Miller, T. W., Sims, C. B., Parsons, G., and Sztenderowicz, M., 2013, "Effect of low viscosity passenger car motor oils on fuel economy engine tests," No. 0148-7191, SAE Technical Paper.
5. Russell, P. A., Morton, T. D., Jackson, L., and Prince, A. S., 2012, 12. Motor engineering knowledge for marine engineers, Bloomsbury Publishing.
6. Hussain, J., Palaniradja, K., Alagumurthi, N., and Manimaran, R., 2012, "Effect of exhaust gas recirculation (EGR) on performance and emission characteristics of a three cylinder direct injection compression ignition engine," Alexandria Engineering Journal, 51(4), pp. 241-247.
7. Hsieh, W.-D., Chen, R.-H., Wu, T.-L., and Lin, T.-H., 2002, "Engine performance and pollutant emission of an SI engine using ethanol-gasoline blended fuels," Atmospheric Environment, 36(3), pp. 403-410.
8. Thring, R., 1983, "Alternative fuels for spark ignition engines," Southwest Research Institute.
9. Wagner, T., Gray, D., Zarah, B., and Kozinski, A., 1980, "Practicality of alcohols as motor fuel," SAE Prog. Technol.:(United States), 19.
10. Kabasin, D., Hoyer, K., Kazour, J., Lamers, R., and Hurter, T., 2009, "Heated injectors for ethanol cold starts," SAE International Journal of Fuels and Lubricants, 2(1), pp. 172-179.
11. Fursund, K., 1957, "Wear in cylinder liners," Wear, 1(2), pp. 104-118.
12. Lakshminarayanan, P. A., and Nayak, N. S., 2011, Critical Component Wear in Heavy Duty Engines, John Wiley & Sons.
13. Neale, M. J., 2001, Lubrication and reliability handbook, Newnes.
14. Williams, C., 1936, "Cylinder wear in gasoline engines," SAE Technical Paper.
15. Hutchings, I. M., 1992, "Tribology: friction and wear of engineering materials."
16. Bisson, E. E., Johnson, R. L., Swikert, M. A., and Godfrey, D., 1956, "Friction, wear, and surface damage of metals as affected by solid surface films," NACA Report 1254, pp. 91-111.
17. Terheci, M., Manory, R. R., and Hensler, J. H., 1995, "The friction and wear of automotive grey cast-iron under dry sliding conditions. Part 1: Relationships between wear loss and testing parameters," Wear, 180(1-2), pp. 73-78.
18. Andersson, P., Tamminen, J., and Sandström, C.-E., 2002, "Piston ring tribology. A literature survey," VTT Tiedotteita - Research Notes 2178. 105 p.

19. Kennedy, F. E., 1984, "Thermal and thermomechanical effects in dry sliding," *Wear*, 100(1-3), pp. 453-476.
20. Kennedy, F. E., Frusescu, D., and Li, J. Y., 1997, "Thin film thermocouple arrays for sliding surface temperature measurement," *Wear*, 207(1-2), pp. 46-54.
21. Kennedy, F., 2001, "Frictional heating and contact temperatures," *Modern tribology handbook*, 1, pp. 235-259.
22. Sutter, G., and Ranc, N., 2010, "Flash temperature measurement during dry friction process at high sliding speed," *Wear*, 268(11-12), pp. 1237-1242.
23. Jaeger, J. C., 1943, "Moving sources of heat and the temperature at sliding contacts," *Proceedings of the Royal Society of New South Wales*, pp. 203-224.
24. Archard, J., 1959, "The temperature of rubbing surfaces," *Wear*, 2(6), pp. 438-455.
25. Blau, P. J., 2008, *Friction science and technology: from concepts to applications*, CRC press.
26. Bergseth, E., Sjoberg, S., and Bjorklund, S., 2012, "Influence of real surface topography on the contact area ratio in differently manufactured spur gears," *Tribology International*, 56, pp. 72-80.
27. Kalin, M., 2004, "Influence of flash temperatures on the tribological behaviour in low-speed sliding: a review," *Materials Science and Engineering: A*, 374(1), pp. 390-397.
28. Kalin, M., and Vižintin, J., 2001, "Comparison of different theoretical models for flash temperature calculation under fretting conditions," *Tribology International*, 34(12), pp. 831-839.
29. Pimenta, M., Dresselhaus, G., Dresselhaus, M. S., Cancado, L., Jorio, A., and Saito, R., 2007, "Studying disorder in graphite-based systems by Raman spectroscopy," *Physical chemistry chemical physics*, 9(11), pp. 1276-1290.
30. Tuinstra, F., and Koenig, J. L., 1970, "Raman spectrum of graphite," *The Journal of Chemical Physics*, 53(3), pp. 1126-1130.
31. Wang, Y., Alsmeyer, D. C., and McCreery, R. L., 1990, "Raman-spectroscopy of carbon materials - Structural basis of observed spectra," *Chemistry of Materials*, 2(5), pp. 557-563.
32. Kerwin, J., Sha, X., and Jackson, B., 2006, "Classical studies of H atom trapping on a graphite surface," *The Journal of Physical Chemistry B*, 110(38), pp. 18811-18817.
33. Robertson, J., 2002, "Diamond-like amorphous carbon," *Materials Science and Engineering: R: Reports*, 37(4), pp. 129-281.
34. Chu, P. K., and Li, L., 2006, "Characterization of amorphous and nanocrystalline carbon films," *Materials Chemistry and Physics*, 96(2), pp. 253-277.
35. Condeço, J., Christensen, L. H., and Rosen, B. G., 2001, "Software relocation of 3D surface topography measurements," *International Journal of Machine Tools & Manufacture*, 41(13-14), pp. 2095-2101.
36. Sudarshan, T. S., and Bhaduri, S. B., 1983, "Wear in cylinder liners," *Wear*, 91(3), pp. 269-279.
37. GOETZE, 2003, "GOETZE® Piston Ring Handbook," <http://koriahandbook.federalmogul.com/en/index.htm>.
38. Barrau, O., Boher, C., Vergne, C., Rezai-Aria, F., and Gras, R., "Investigations of friction and wear mechanisms of hot forging tool steels," *Proc. 6th International Tooling Conference*, pp. 81-94.

## Contact Information

Rafael Brisolla Obara

TUPY S.A. – Research, Development and Innovation  
 Email: rafael.obara@tupy.com.br  
 URL: www.tupy.com.br